Earthquake Engineering, Tenth World Conference © 1992 Balkema, Rotterdam. ISBN 90 5410 060 5

Testing of full scale shear wall structures under seismic load

A. Igarashi, F. Seible & G.A. Hegemier
University of California, San Diego, Calif., USA

ABSTRACT: A full-scale testing procedure with an on-line computer controlled multi-actuator system was developed and implemented for the testing of stiff shear wall type structures. The test method was implemented and verified on 3-story full scale reinforced masonry shear walls and is currently enhanced to test a 5-story full scale reinforced masonry research building under simulated seismic loads at the university of California, San Diego. The paper discusses characteristics improvements for the outlined test procedure.

1 INTRODUCTION

A large number of new design models and complex nonlinear analysis codes have been developed in the academic research environment over the past years to predict the realistic response of structures under earthquake loads at various limit states such as yield, maximum capacity and ultimate collapse. Due to the limited availability of field data, the quality and usefulness of these models depends to a large extent on their verification and calibration through laboratory experiments. These laboratory tests need to be performed on a large or full scale in order to capture the correct development of local and global failure modes. Thus, experimental techniques are needed which allow realistic seismic load input to full-scale structural systems. This realistic seismic load input should consist of recorded or synthetic ground acceleration time histories, simulate the mass proportional nature of inertia type loads and reflect the nonlinear dynamic characteristics of the structure in terms of stiffness degradation and higher mode effects. Since shake table tests are limited in scope by payload size and weight, reaction wall tests with on-line computer controlled multiple actuator systems have been developed which apply seismic load input through a pseudo-dynamic sequentially quasi-static scheme utilizing predicted structural displacements from analytical models and time integration schemes of various complexity.

Problems with pseudo-dynamic full-scale tests of stiff multi-degree-of-freedom structures to date consisted of (1)spurious higher mode effects leading to error growth and loading system instabilities, (2)stiff coupling between actuators leading to convergence problems, and (3)unrealistic simulation of mass proportional loads through concentrated point loads or loading system constraining effects. In an effort to adopt a pseudo-dynamic test methodology to the full-scale testing of stiff structures such as a reinforced concrete masonry 5-story coupled shear wall research building shown in Figure 1, research developments focused on mass proportional loading systems with controlled soft coupling, controlled experimental displacement error growth, and experimental procedures which do not require artificial numerical damping in order to suppress spurious higher mode

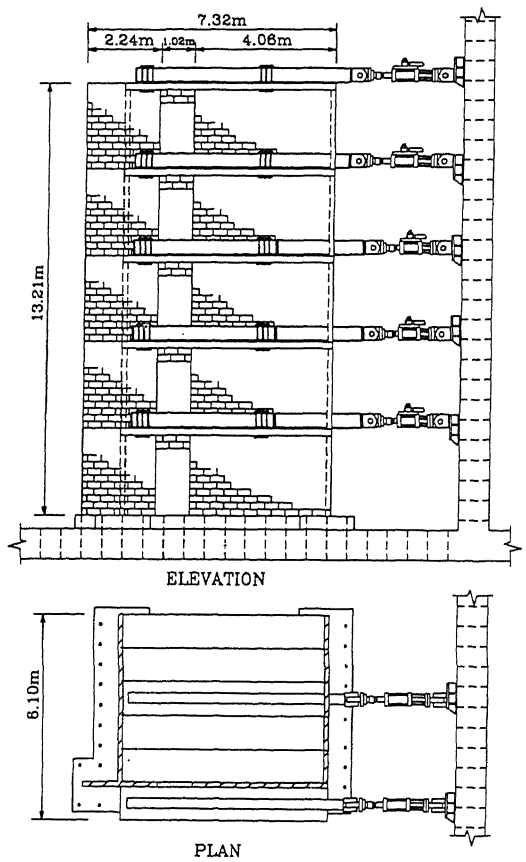

Figure 1. 5-story building test setup.

effects. The evolving test methodology, termed GSD (Generated Sequential Displacement procedure) is discussed in the following, together with implementation and verification on three-story full scale shear wall specimens and extensions to enhance the convergence characteristics for the upcoming 5-story full scale building test.

2 TEST METHODOLOGY

The GSD procedure is based on the pseudo dynamic testing principle (Mahin *et al.* 1989) where parallel analytical and experimental models are used interactively to trace the nonlinear response of a structure to a seismic load input. While structural deterioration and stiffness degradation are measured as restoring forces on the test floor, the seismic deformations for the next time step are determined in the analytical model and subsequently applied to the test specimen. Therefore, it is essential for a successful pseudo dynamic test to accurately impose and monitor structural displacements. Relevant hardware and software requirements are discussed in the following.

The hardware components of the loading system consist of the servo controlled actuators, load distribution beams connected to the actuators and elastomeric bearing pads which transmit the load to the test specimen. As an example, the test setup, geometry and dimensions of a three-story shear wall used in the first series of GSD implementation experiments is shown schematically in Figure 2. In this setup, the loads were transmitted to the structure at each floor slab through load distribution beams and two elastomeric bearing pads.

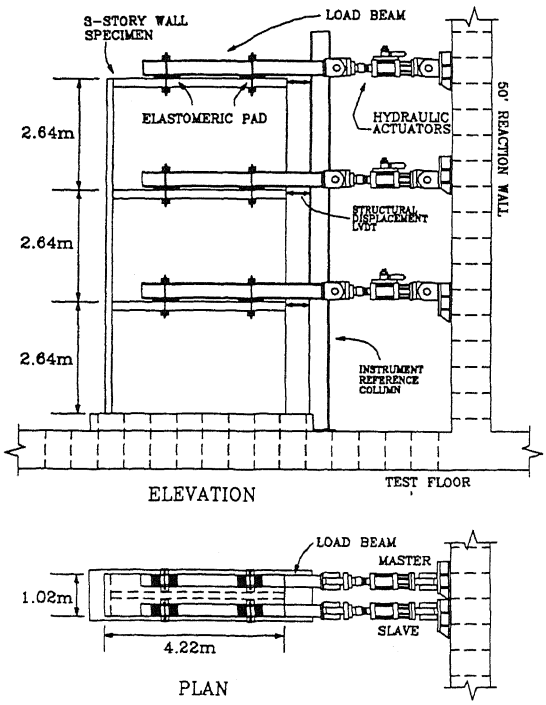

Figure 2. 3-story wall test setup and dimensions.

2.1 Elastomeric pads

The idea behind the use of elastomeric pads is that they act as (a) equal load distributors, and (b) soft springs between actuators and the specimen (structure). The first feature provides a mass-proportional loading to the specimen, and limited unconstrained structural rotations and expansions of the floor system, thus allowing structural deterioration without compromising the mass proportional loading. The second feature, which is illustrated in Figure 3, on a 2-DOF system, improves the displacement control of the structure at small displacement levels through displacement amplification, and also protects the structure from actuator instabilities during shake down testing. The mechanical displacement amplification from this soft spring effect of the elastomeric pads is discussed in the next section.

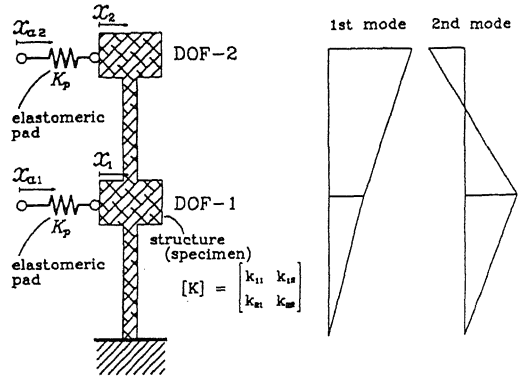

Figure 3. Linear 2-DOF model.

2.2 Displacement amplification

In the following, symbols with hat (^) refer to "actually measured" or "experimental" values, while symbols without hat represent values which are "computed" or "idealized". Consider a structure with n degrees of freedom, and the actuator displacements as an n-dimensional vector $\mathbf{x}_a$ and structural displacements as an n-dimensional vector $\mathbf{x}$. Let us assume that the actuators cannot be controlled precisely, resulting in an actuator displacement error $\hat{\mathbf{x}}_a - \mathbf{x}_a$ with an actuator displacement error bound δ of the form

$$\|\hat{\mathbf{x}}_a - \mathbf{x}_a\| \leq \delta \tag{1}$$

where $\mathbf{x}_a$ is the calculated actuator displacement vector or command signals, and $\|\cdot\|$ represents the norm of a vector. The value of the actuator displacement error bound is dependent on the servo controlled actuator system and cannot be zero. If the actuators are directly connected to the specimen without elastomeric pads, the (experimental) structural displacement vector $\hat{\mathbf{x}}$ will be such that

$$\|\hat{\mathbf{x}} - \mathbf{x}\| \leq \delta \tag{2}$$

This implies that the error bound for the structural displacement is also δ , i.e. the precision of the structural displacements is equal to the precision of the actuator displacements.

Now, consider the case in which the specimen and the actuators are connected through elastomeric pads. This situation is described by the model shown in Figure 3. The actuator displacement vector and the structural displacement vector are related by

$$\hat{\mathbf{x}}_a = \mathbf{Q}\hat{\mathbf{x}} \tag{3}$$

where $\mathbf{Q}$ is an $n \times n$ "displacement amplification matrix", which can be expressed by

$$\mathbf{Q} = \mathbf{I} + \frac{1}{K_p}\mathbf{K} \tag{4}$$

where K_p is the elastomeric pad stiffness, $\mathbf{K}$ is the stiffness matrix of the structure. Since

$$\hat{\mathbf{x}} - \mathbf{x} = \mathbf{Q}^{-1}(\hat{\mathbf{x}}_a - \mathbf{x}_a) \tag{5}$$

the structural displacement error can be bounded as follows:

$$\begin{aligned} \|\hat{\mathbf{x}} - \mathbf{x}\| &\le \|\mathbf{Q}^{-1}\|_2 \|\hat{\mathbf{x}}_a - \mathbf{x}_a\| \\ &\le \|\mathbf{Q}^{-1}\|_2 \cdot \delta \end{aligned} \tag{6}$$

where $\|\cdot\|_2$ denotes the two-norm of a matrix (Gill *et al.* 1991). If the stiffness matrix $\mathbf{K}$ is positive definite, the matrix $\mathbf{Q}^{-1}$ is also positive definite, and in this case, the two-norm of the matrix $\mathbf{Q}^{-1}$ is simply the largest eigenvalue of $\mathbf{Q}^{-1}$, i.e.

$$\|\mathbf{Q}^{-1}\|_2 = \left\| \Phi \, \mathrm{diag}\left(\frac{1}{1+\frac{\lambda_1}{K_p}}, \ldots, \frac{1}{1+\frac{\lambda_n}{K_p}} \right) \Phi^T \right\|_2$$

$$= \frac{1}{1+\frac{\lambda_1}{K_p}} \tag{7}$$

where λ_i is the eigenvalue of the stiffness matrix $\mathbf{K}$ for the ith mode, and Φ is the matrix consisting of eigenvectors φ_i such that $\mathbf{K}\varphi_i = \lambda_i \varphi_i$ and $\|\varphi_i\| = 1$. Note that these eigenvectors coincide with the dynamic mode shapes if the lumped mass is equally distributed to all the DOFs. Therefore,

$$\|\hat{\mathbf{x}} - \mathbf{x}\| \le \frac{\delta}{1+\frac{\lambda_1}{K_p}} \tag{8}$$

This result indicates that by using a small elastomeric pad stiffness K_p , the structural displacement error vector $\hat{\mathbf{x}}-\mathbf{x}$ can be made smaller than the actuator precision.

It can also be shown that the elastomeric pads lessen the restoring force error resulting from the inaccurate actuator displacement, and reduce the coupling between structural DOFs, thus almost eliminating spurious higher order interaction effects during initial load stages at which the structure is undamaged and stiff.

There is a danger that the actuators reach their stroke limit with this displacement amplification. However, with the small elastomeric pad thickness of 1/2" used for the tests shown in Figure 2, higher amplification is obtained at low load levels when displacements are very small, while the amplification effect decreases with increasing loads due to deformation constraint in the elastomeric pads at strain levels exceeding 100%.

2.3 Software: inner control loop

Although the introduction of the elastomeric pads provides the discussed advantages for stiff multi-degree-of-freedom system, it also adds complications to the actuator control algorithm, see Figure 4. For a

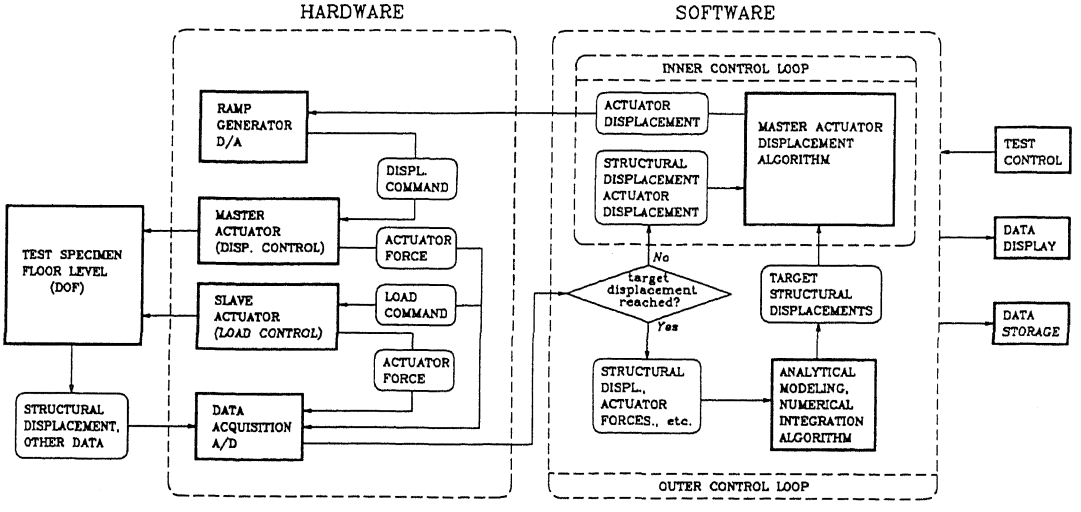

Figure 4. Test system diagram (per floor level).

highly nonlinear test structure, it is difficult to obtain the actuator displacement which results in the target structural displacement specified by the pseudo-dynamic algorithm. An iterative procedure to search for the appropriate actuator displacement vector needs to be implemented. In order to allow such a procedure, the testing system is configured as shown in Figure 4.

The inner control loop algorithm used in the three-story wall test can be described as follows: After the structural displacement measurements are compared in a software control loop with calculated target displacement levels, the structural displacement increments to be imposed is obtained. This increment is then appropriately scaled (to improve convergence and test speed) and used as the next actuator displacement increment.

This inner loop algorithm can be expressed by either

$$x_a^{(k+1)} = \hat{x}_a^{(k)} + \nu\left(x_{target} - \hat{x}^{(k)}\right), \quad k=0,1,... \tag{9}$$

or

$$x_a^{(k+1)} = x_a^{(k)} + \nu\left(x_{target} - \hat{x}^{(k)}\right), \quad k=0,1,... \tag{10}$$

with k denoting the inner loop iteration step and ν the displacement increment scale factor. Both algorithms were tested, and it was found that the algorithm (10) provided faster convergence and less structural displacement error than (9), since the relation between the command signal ($x_a^{(k)}$) and the actuator displacement ($\hat{x}_a^{(k)}$) is possibly off-bias and not completely linear.

2.4 Software: outer control loop

Several time integration schemes, such as Newmark explicit, modified Newmark explicit, and the Hilber's alpha method with initial stiffness iteration were implemented in the outer control loop. Also, a restoring force correction scheme (Nakashima & Kato 1987) was added to the outer loop. At time step i, in the outer loop calculation of the next target displacement $x_{target}(i+1)$, a "corrected" restoring force

$$\bar{r}(i) = \hat{r}(i) + \hat{K}_0\left(x_{target}(i) - \hat{x}(i)\right) \tag{11}$$

is used instead of the measured restoring force $\hat{r}(i)$. In eqn.(11), $\hat{K}_0$ is the initial structural stiffness measured experimentally at the beginning of the test segments. The application of this outer loop restoring force correction scheme in conjunction with the implicit Hilber's alpha method was reported by (Shing *et al.* 1991). The proposed GSD for the first U.S. 5-story full scale building test will implement a similar scheme as a modification to the inner control loop (Seible *et al.* 1991).

3 RESULTS OF THREE-STORY SHEAR WALL TESTS

Some results from the three-story full-scale masonry wall tests with the methodology explained above are presented in the following. For comparison of the effect of the different time integration schemes, tests are performed using the stiff pre-yield state of one of the wall specimens. The input acceleration used was a sequence of time windows from a record of Imperial Valley (1979) earthquake. Obtained displacement response time-histories for the three tests are depicted in Figure 5. As can be seen, Test 19, the modified Newmark explicit (MNE) scheme (Figure 5a) resulted in a first mode response, since all higher mode effects were numerically damped out. Some higher mode effects were captured with Hilber's alpha (HA) method

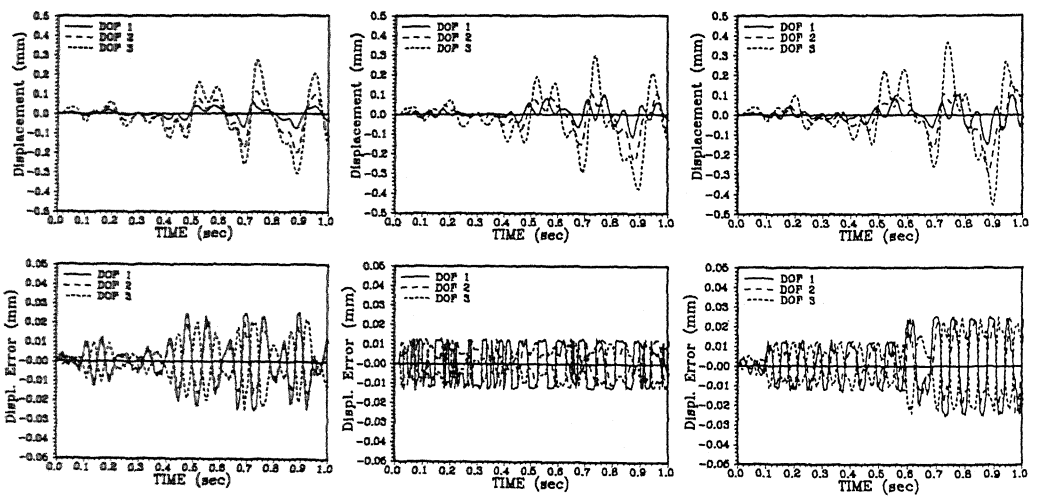

(a) Test 19 (MNE) (b) Test 20 (HA) (c) Test 21 (NE)

Figure 5. Structural displacement and displacement error histories for 3-story wall tests.

(Test 20), with 5% damping per mode. This higher mode response is visible in Figure 5b in the displacement time-history and in the increased restoring forces. Finally, the Newmark explicit (NE) scheme, without any numerical damping, featured the largest second mode contributions, as can be seen in Figure 5c. The displacement error can be tightly controlled by specified error tolerances (note the three different levels in Figure 5c), where the error tolerance was adjusted in three steps.

The above discussed modifications to conventional on-line testing techniques have allowed the testing of stiff masonry wall systems with GSD, using reliable integration schemes such as NE without introducing artificial numerical damping. Pseudo-dynamic test rates were one to four thousand times the real seismic event, resulting in test durations of typically less than one hour per one second of earthquake time-history. Further development to improve on the test speed are discussed in the following.

4 CONVERGENCE ANALYSIS

It can be shown that the convergence of the structural displacement to the target displacement is obtained when the inner control loop algorithm is given by expression (9) or (10). For simplicity of the analysis, it is assumed that the system is linear ($\mathbf{K}$, K_p), and that

$$\hat{\mathbf{x}}_a^{(k)} = \mathbf{x}_a^{(k)} \tag{12}$$

for all iteration steps k. This implies that the actuators perfectly follow the displacement command signals. Then the algorithm (9) or (10) result in the following equation:

$$\mathbf{x}_a^{(k+1)} = \mathbf{x}_a^{(k)} + \nu\left(\mathbf{x}_{target} - \mathbf{x}^{(k)}\right), \quad k=0,1,... \tag{13}$$

where ν is a scalar multiplier such that $\nu>1$, $\mathbf{x}_{target}$ is the structural displacement vector to be achieved, $\mathbf{x}_a^{(k)}$ and $\mathbf{x}^{(k)}$ are the actuator and structural displacement vector at iteration step k, respectively.

Assume a linear system as above, and substituting (3) and (4) in (13), a difference equation for the structural displacement is obtained as

$$\mathbf{x}^{(k+1)} = (\mathbf{I}-\nu\mathbf{Q}^{-1})\mathbf{x}^{(k)} + \nu\mathbf{Q}^{-1}\mathbf{x}_{target} \qquad k=0,1,... \tag{14}$$

along with the initial condition, $\mathbf{x}^{(0)}$.

If the target structural displacement vector $\mathbf{x}_{target}$ is constant during the iteration, this difference equation is solved in the following manner. The equation is rearranged to the form

$$\mathbf{x}_{target} - \mathbf{x}^{(k+1)} = (\mathbf{I}-\nu\mathbf{Q}^{-1})\left(\mathbf{x}_{target} - \mathbf{x}^{(k)}\right) \tag{15}$$

Hence, if

$$\mathbf{u}^{(k)} = \mathbf{x}_{target} - \mathbf{x}^{(k)} , \quad k=0,1,... \tag{16}$$

is defined, it is easy to show that the solution of eqn. (14) is given by

$$\mathbf{u}^{(k)} = (\mathbf{I}-\nu\mathbf{Q}^{-1})^k \mathbf{u}^{(0)} \quad k=0,1,... \tag{17}$$

Since the matrix $\mathbf{Q}$ has the same eigenvectors as the stiffness matrix $\mathbf{K}$, and the corresponding eigenvalues are $1+\lambda_i/K_p$ (λ_i = the eigenvalue of $\mathbf{K}$), the solution can be decomposed into modes using the eigenvectors of the stiffness matrix, as

$$w_i^{(k)} = \mu^k w_i^{(0)} , \quad k=0,1,... \tag{18}$$

where $w_i^{(k)}$ is the ith mode component in the vector $\mathbf{u}^{(k)}$, and

$$\mu_i = 1 - \frac{\nu}{1+\frac{\lambda_i}{K_p}}, \quad i=1,2,...,n \tag{19}$$

Therefore, if $|\mu_i|<1$ (preferably $0\le\mu_i<1$), all the components of $\mathbf{u}^{(k)}$ converge to zero as $k\to\infty$. The numbers μ_i (i=1,2,...,n) correspond to the rate of convergence of the structural displacement to the target displacement in the ith mode. As can be seen in the above expression, μ_i is larger for a higher mode (with larger λ_i), thus the convergence is slower.

As an example, Figure 6 illustrates the convergence behavior of the 2-DOF model shown in Figure 3. Several simulated structural displacement paths are shown, starting from different initial structural displacements. Only the first seven iterated points are shown in the figure. In the two degrees of freedom displacement domain shown in Figure 6, convergence along a positive slope corresponds to dominant first mode response while convergence along a negative slope indicates dominance of second mode contribution. In Figure 6, it can be seen that the second mode (the highest mode in this case) becomes dominant in the displacement error vector near the

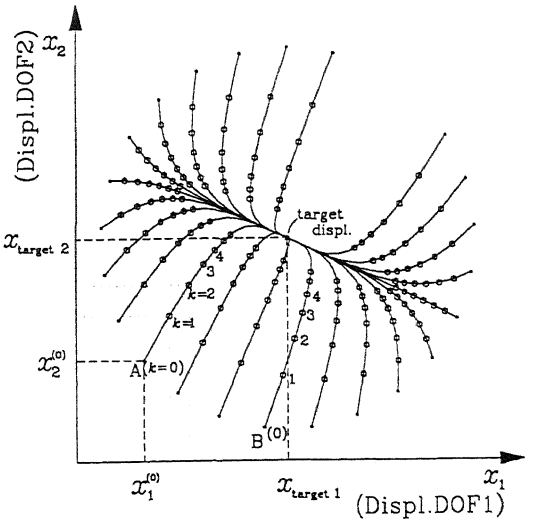

Figure 6. Convergence behavior of 2-DOF model.

target displacement point. Also, overshooting of individual DOFs can be observed which slows down the convergence behavior.

5 FUTURE IMPROVEMENT

Since the higher mode converges slower than other modes, as shown in the previous section, the residual structural displacement error at the end of the inner loop iteration will contain predominant highest mode components. This may induce unrealistically large highest mode response, and it also significantly slows down the speed of convergence.

Hence, one of improvements considered to the inner control loop algorithm is to compensate the slow convergence of higher modes. In order to accomplish this, the inner control loop algorithm takes on the form

$$x_a^{(k+1)} = x_a^{(k)} + N\left(x_{target} - \hat{x}^{(k)}\right) \tag{20}$$

where N is an $n \times n$ scaling matrix. By choosing the value of N , the convergence properties of the algorithm can be controlled. The algorithm used in the three-story wall tests can be treated as a special case where

$$N = \nu I \tag{21}$$

In the above 2-DOF linear system example, if the matrix Q is known through measurements, the choice

$$N = \hat{u} Q \tag{22}$$

where $\hat{u}$ is a reduction factor, gives the structural displacement paths shown in Figure 7. Note that all the modes have the same convergence rate in this case, and no overshooting is encountered.

These latest improvements to the inner loop algorithm of the GSD procedure are currently implemented and tested in preparation for the 5-story full scale masonry research building test. Due to the stiff nature of the proposed 5-story research building, explicit integration schemes would require severe restrictions on the time step to maintain numerical stability, thus, implicit integration schemes with the discussed error correction will be implemented (Seible *et al.* 1991).

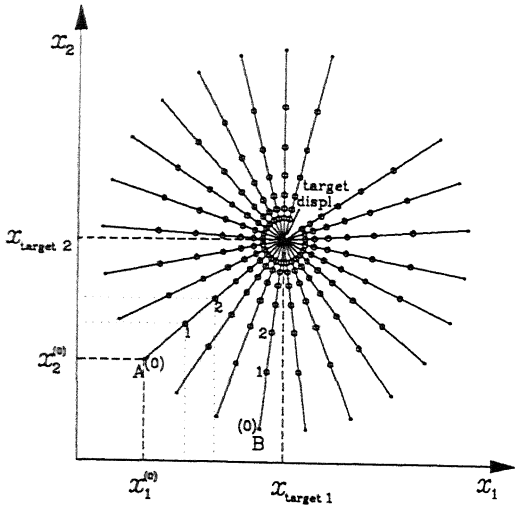

Figure 7. Convergence of 2-DOF model with improved algorithm.

6 CONCLUSIONS

It can be shown that the extensions to the pseudo dynamic testing procedure implemented in GSD result (1) in stable test procedures without artificial damping, (2) in full participation of higher mode effects, (3) in more realistic mass proportional loadings, and (4) in significantly improved overall pseudo-dynamic test speed. Results from the full-scale tests of three-story shear wall structures showed that the developed test method can be successfully applied even in the initial or stiff undamaged structural state. The developed procedure will now be applied to the first U.S. five-story full-scale building test under simulated seismic loads.

ACKNOWLEDGEMENT

The present research is supported by the National Science Foundation under Grant No. BCS-9102430.

REFERENCES

Gill,P.E., W.Murray & M.H.Wright. 1991. *Numerical linear algebra and optimization, Vol.1*. Redwood City, California: Addison-Wesley.

Mahin,S.A., P.B.Shing, C.R.Thewalt & R.D.Hanson. 1989. Pseudodynamic test method - current status and future directions. *Journal of structural engineering*, Vol.115, No.8: 2113-2128. ASCE.

Nakashima,M. & H.Kato. 1987. *Experimental error growth behavior and error growth control in on-line computer test control method.* #123. Tsukuba: BRI.

Seible,F. & A.Igarashi. 1991. Full scale testing of masonry structures under simulated seismic loadings. *Experimental and numerical methods in earthquake engineering*(Donea,J. and P.M.Jones eds.): 119-148. Brussels & Luxemburg.

Seible,F., M.J.N.Priestley, G.A.Hegemier, G.R. Kingsley, A.Igarashi & A.G.Kurkchubasche. 1991. *The test plan for the 5-story full-scale TCCMAR research building.* SSRP-91/07. Univ. of Calif., San Diego, Dept. of AMES.

Shing,P.B., M.T.Vannan & E.Carter. 1991. Implicit time integration for pseudodynamic tests. *Earthquake engineering and structural dynamics*, Vol.20: 551-576.